Interseismic Deformation Associated with Three-Dimensional Faults in the Greater Los Angeles Region, California

Scott T. Marshall - (marshall@geo.umass.edu)
Michele L. Cooke - (cooke@geo.umass.edu)
Susan E. Owen - (Susan.E.Owen@jpl.nasa.gov)

ABSTRACT

We introduce a methodology for simulating interseismic deformation along multiple interacting non-parallel faults. We show that the analytical solution for surface displacement associated with slip on a semi-infinite vertical strike-slip fault is identical to that of a vertical fault of finite vertical width that joins at depth with two horizontal dislocations with opposite senses of displacement. Based on this analytical solution, we formulate a two-step approach for the numerical investigation of geologic and interseismic deformation that allows three-dimensional fault surfaces to interact and accumulate mechanically and kinematically viable slip distributions. We apply this approach to the complex network of faults in the Los Angeles region and find that the geologic model results match well geologic slip rate data and the interseismic model results match well the heterogeneous GPS velocity pattern in the Los Angeles region. Heterogeneous interseismic deformation produced by our three-dimensional model implies that two-dimensional analyses of the Los Angeles region cannot sufficiently simulate neotectonic deformation. The ability of these models to reproduce well both geologic slip rates as well as interseismic geodetic velocities suggests that current-day contraction rates in the greater Los Angeles region are compatible with long term geologic deformation rates and disputes suggestions of temporally variable fault slip rates inferred from existing two-dimensional investigations.

ANALYTICAL INTERSEISMIC MODELS

In order to derive an analytical model that is better suited for finite intersecting faults, we use the solutions of Okada [1985] for finite rectangular dislocations to set up an earthquake cycle model equivalent to the conventional model. The net, fault-parallel displacement field for any number of elementary dislocations can be found by finding the sum of the contributions from each elementary dislocation.

CONVENTIONAL INTERSEISMIC MODEL

For a single vertical fault of infinite length and width located along the x-axis (after simplification), the solution approaches the conventional solution,

$$u_x = \left(\frac{-U}{\pi}\right)\arctan\left(\frac{y}{D}\right)$$

where U_x is the fault-parallel displacement, U is the displacement on the fault, y is the distance from the fault trace, and D is the locking depth.

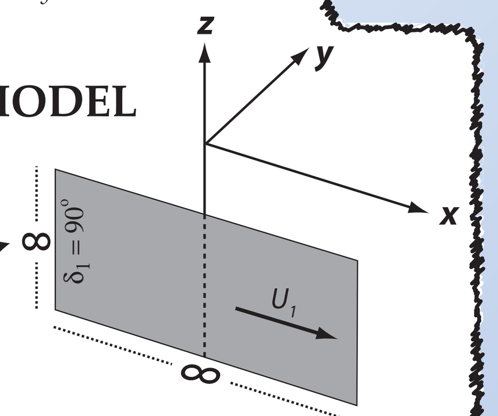

EQUIVALENT EQ CYCLE MODEL

The fault-parallel displacement for a vertical rectangular dislocation of finite width and infinite length is given by

$$u_x = \frac{-U}{\pi}\left[\arctan\left(\frac{y}{D}\right) - \arctan\left(\frac{y}{d}\right)\right]$$

This agrees with existing solutions for a fault of finite height [e.g. Savage, 1980; 1990]. This solution only differs from (1) in that an additional term, –arctan (y/d), is present to account for the finite height of the fault. Therefore, to simulate an infinitely tall fault (i.e. W = ∞) this additional term must be effectively removed.

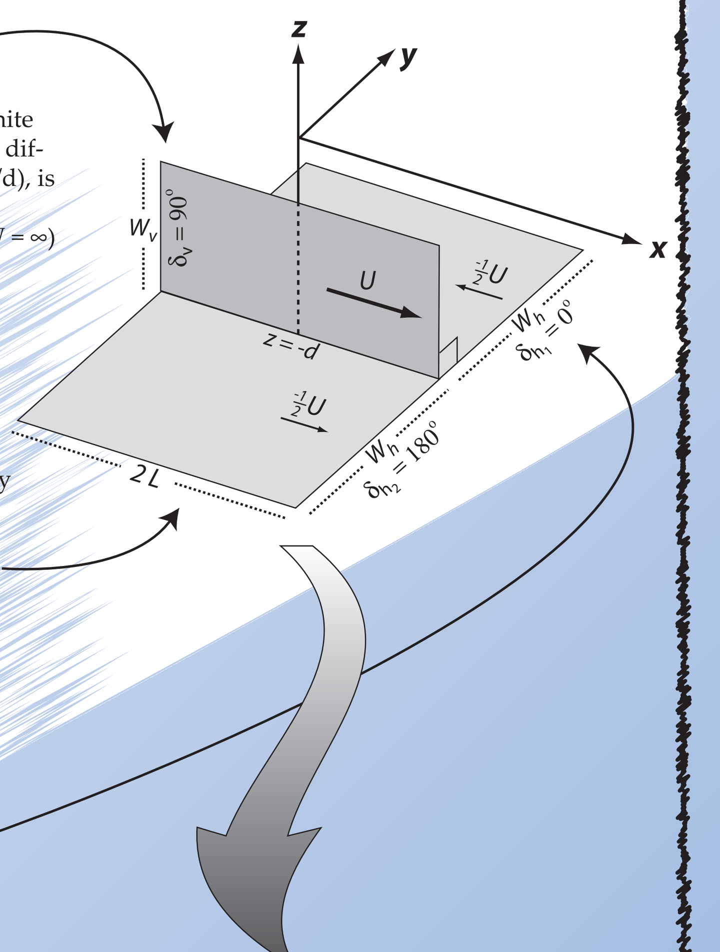

For a horizontal dislocation (δ = 180) the fault-parallel displacement at the free surface is given by

$$u_x = \frac{-U}{2\pi}\left[\arctan\left(\frac{-y}{d}\right) + \frac{\pi}{2}\right]$$

For a horizontal dislocation (δ = 0) with a uniform strike-slip displacement, the fault-parallel displacement at the free surface is given by

$$u_x = \frac{-U}{2\pi}\left[\arctan\left(\frac{-y}{d}\right) - \frac{\pi}{2}\right]$$

Adding the displacement contributions from each of the three dislocations, we arrive at the conventional interseimic solution. Note that this solution is independent of depth to the horizontal detachments.

$$\boxed{u_x = \left(\frac{-U}{\pi}\right)\arctan\left(\frac{y}{D}\right)}$$

NUMERICAL IMPLEMENTATION

1) GEOLOGIC DEFORMATION

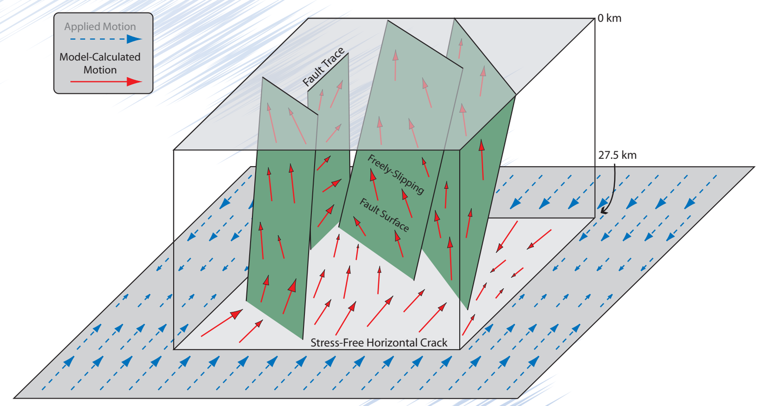

STEP #1 - In the first step, a geologic time scale model is created by allowing the entirety of fault surfaces to freely slip in response to displacements applied at the base of the horizontal detachment.

2) INTERSEISMIC DEFORMATION

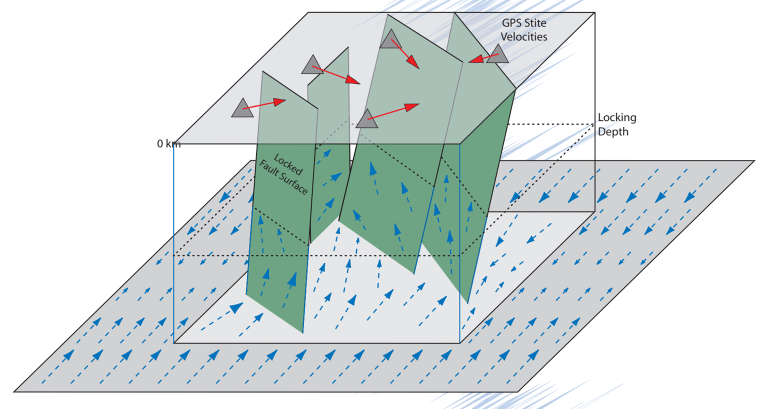

STEP #2 - In the second step, slip from below the locking depth is applied to simulate interseismic deformation (similar to backslip approach). Surface velocities can then be calculated at the locations of GPS sites and compared to existing GPS data.

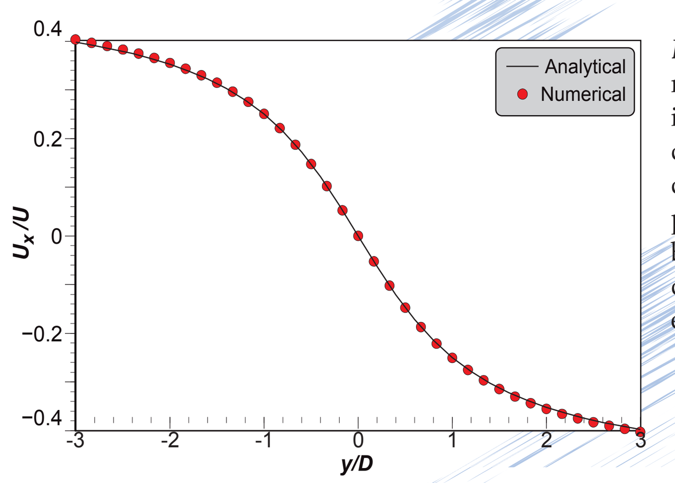

LEFT - Theoretical and BEM model generated fault parallel interseismic displacements. The decoupled BEM model reproduces well the conventional displacement profile. Discrepancies between theory and model predictions reflect discretization errors.

GEOLOGIC MODEL SLIP RATES

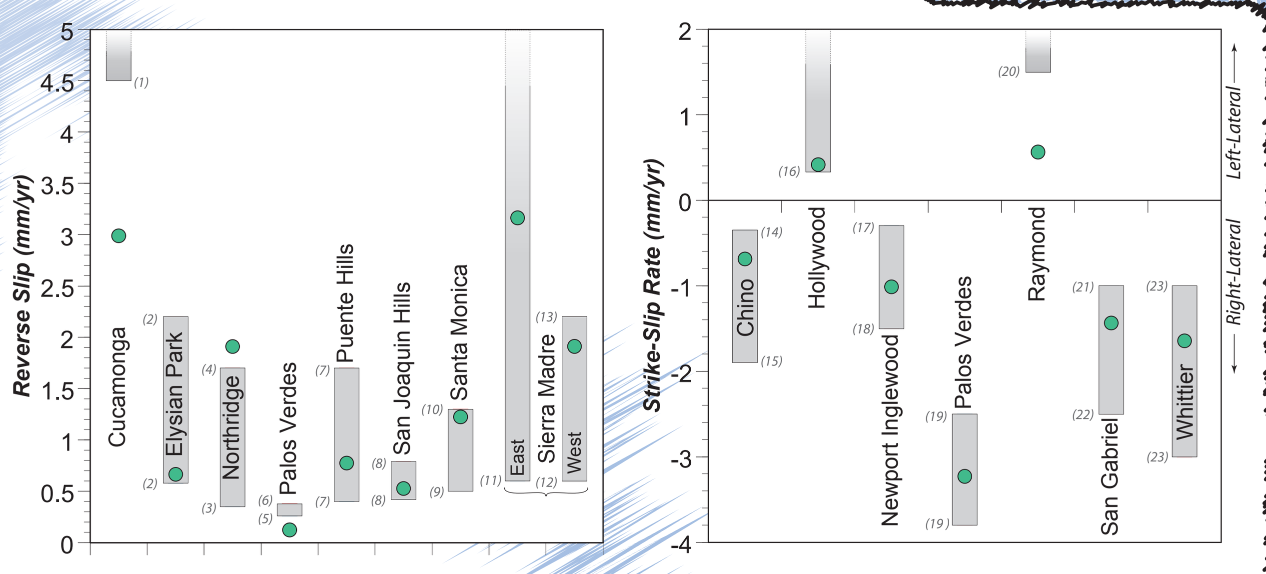

ABOVE - Model-predicted average slip rates (circles) and geologic slip rate estimates (grey ranges). Gradient shading on geologic ranges indicate that the upper limit is poorly constrained. To calculate the average slip rate of modeled fault surface containing many elements of varying size, we integrate the slip over each element's area and calculate a weighted average slip rate for each surface. References for the upper and lower geologic slip rate ranges are shown by gray italic numbers and are as follows: 1) Morton and Matti [1987] 2) Oskin et al. [2000] 3) Dolan et al. [1997] 4) Huftile and Yeats [1996] 5) Bryant [1987] 6) McNeilan et al. [1996] 7) Shaw et al. [2002] 8) Grant et al. [1999] 9) Dolan and Pratt [1997]; Dolan et al. [2000] 10) Tsutsumi et al. [2001] 11) Tucker and Dolan [2001] 12) Rubin et al. [1998] 13) Crook et al. [1987] 14) Walls and Gath [2001] 15) Yeats [2002] 16) Dolan et al. [1997] 17) Freeman et al. [1992]; Grant et al. [1997] 18) Lindvall and Rockwell [1995] 19) Stephenson et al. [1995] 20) Marin et al. [2000] 21) Kahle [1986] 22) Yeats et al. [1994] 23) Gath et al. [1992].

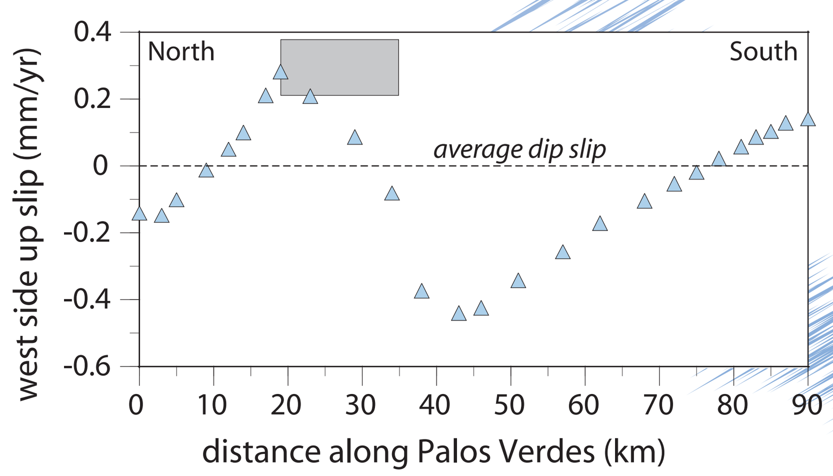

LEFT: West side up slip rate along the vertical Palos Verdes fault. (***From Cooke and Marshall 2006)*** The grey box shows the locations and slip rates determined from analysis of uplifted marine terraces along the Palos Verdes peninsula [Bryant, 1987; Ponti and Lajoie, 1992].

APPLICATION: FAULTS OF THE LA BASIN

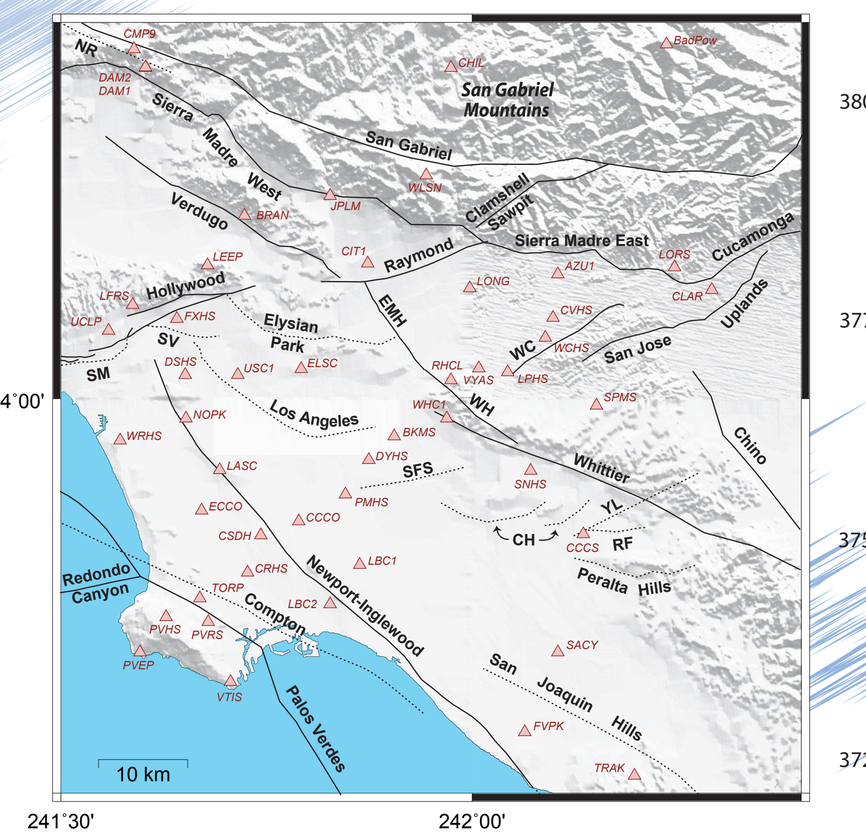

ABOVE - Map showing active fault traces and GPS stations of the greater Los Angeles region. The upper traces of blind faults are indicated by black dashed lines. GPS stations (site names in capital letters) are indicated by triangles.

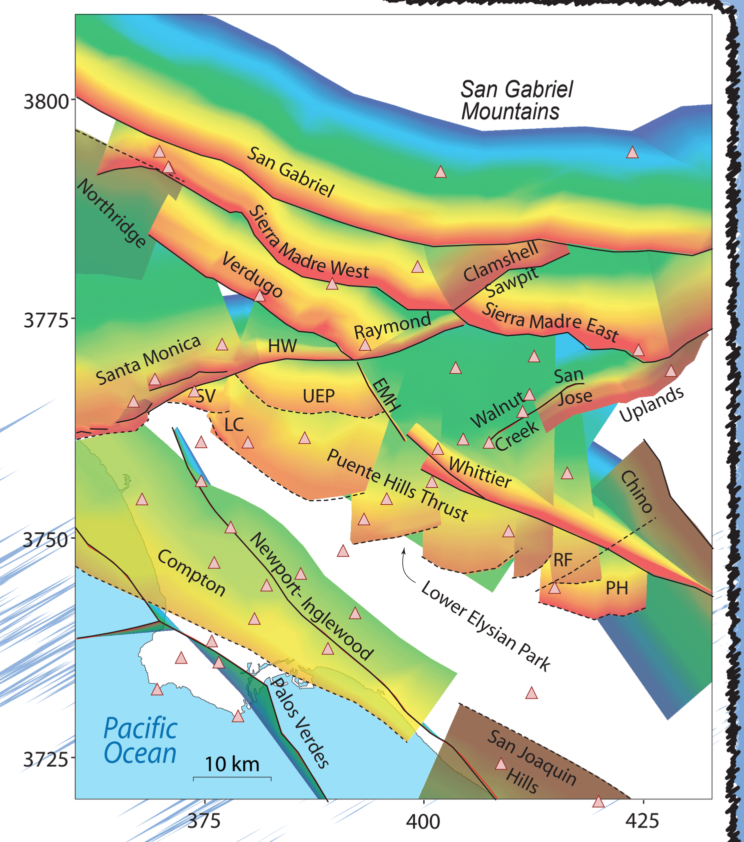

ABOVE - Faults are color shaded by depth : red = surface and dark blue = 27.5 km. This model is based on the SCEC CFM version 2.5. Coordinates are given in UTM (km).

INTERSEISMIC MODELS

LOCKING DEPTH SENSITIVITY

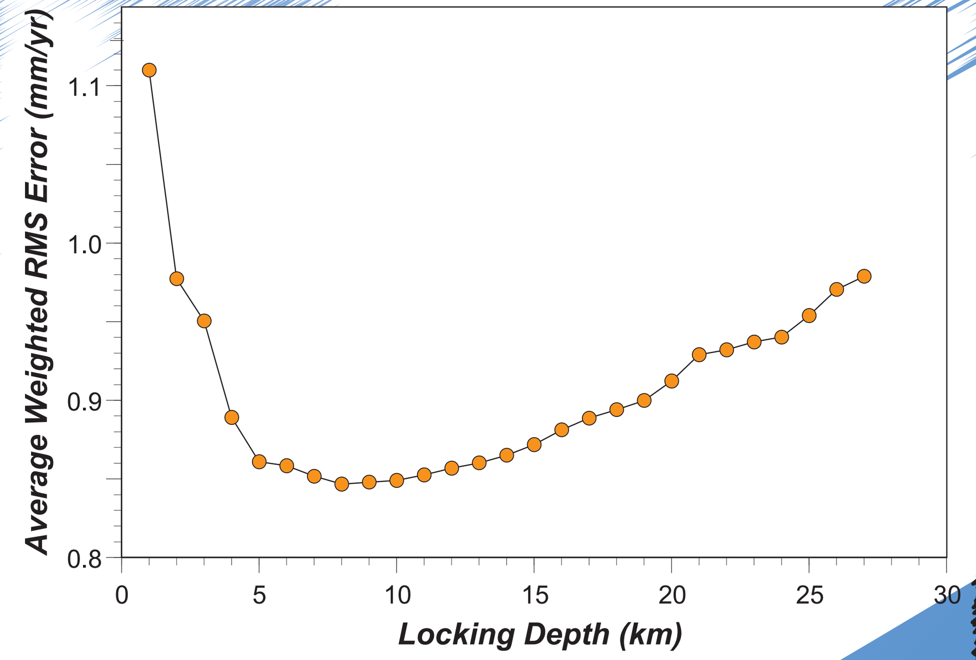

ABOVE: Average weighted residual RMS errors for interseismic models of the Los Angeles region utilizing various locking depths. Although an 8 km locking depth minimizes the weighted RMS error, locking depths of 5-13 km do not provide significantly worse overall match to GPS velocities.

INTERSEISMIC GPS AND MODEL VELOCITIES

BELOW LEFT: GPS velocities from Argus et al. 2005 and model-predicted surface velocities. Model velocities are shown for a locking depth of 8 km.

BELOW RIGHT: GPS-model residual velocities. The four areas of greatest residuals correspond to locations with large non-tectonic ground motions.

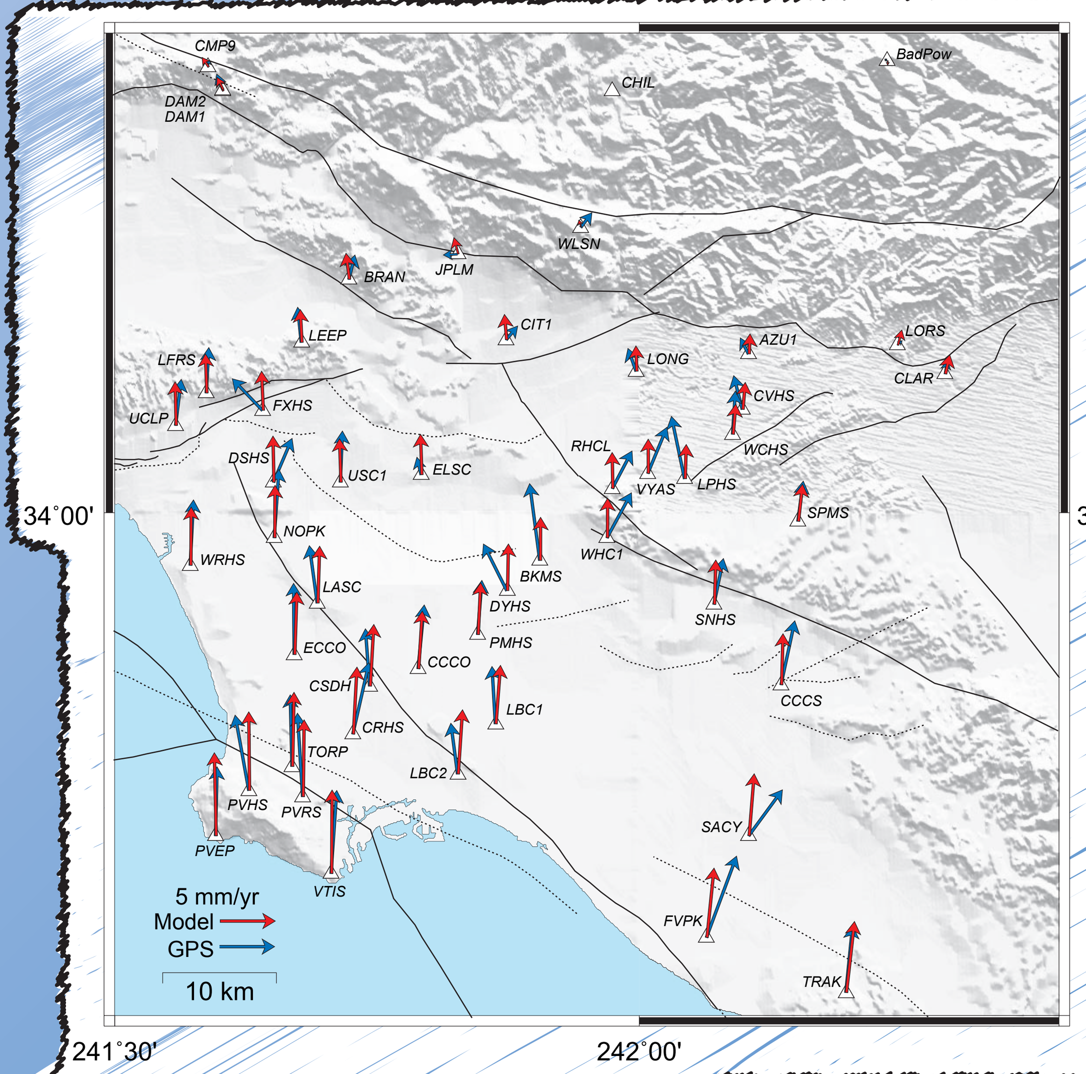

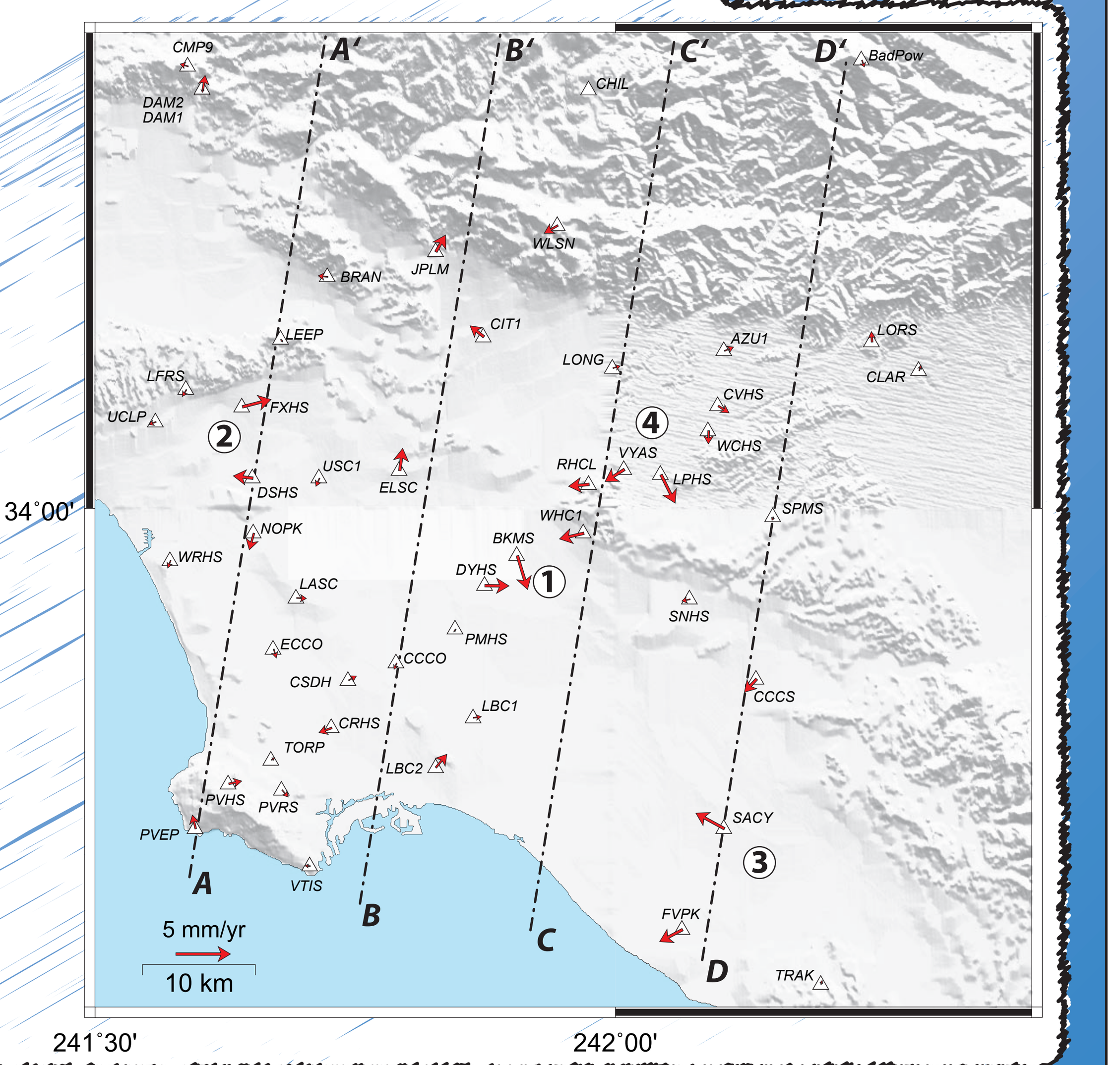

MODEL AND GPS TRANSECTS

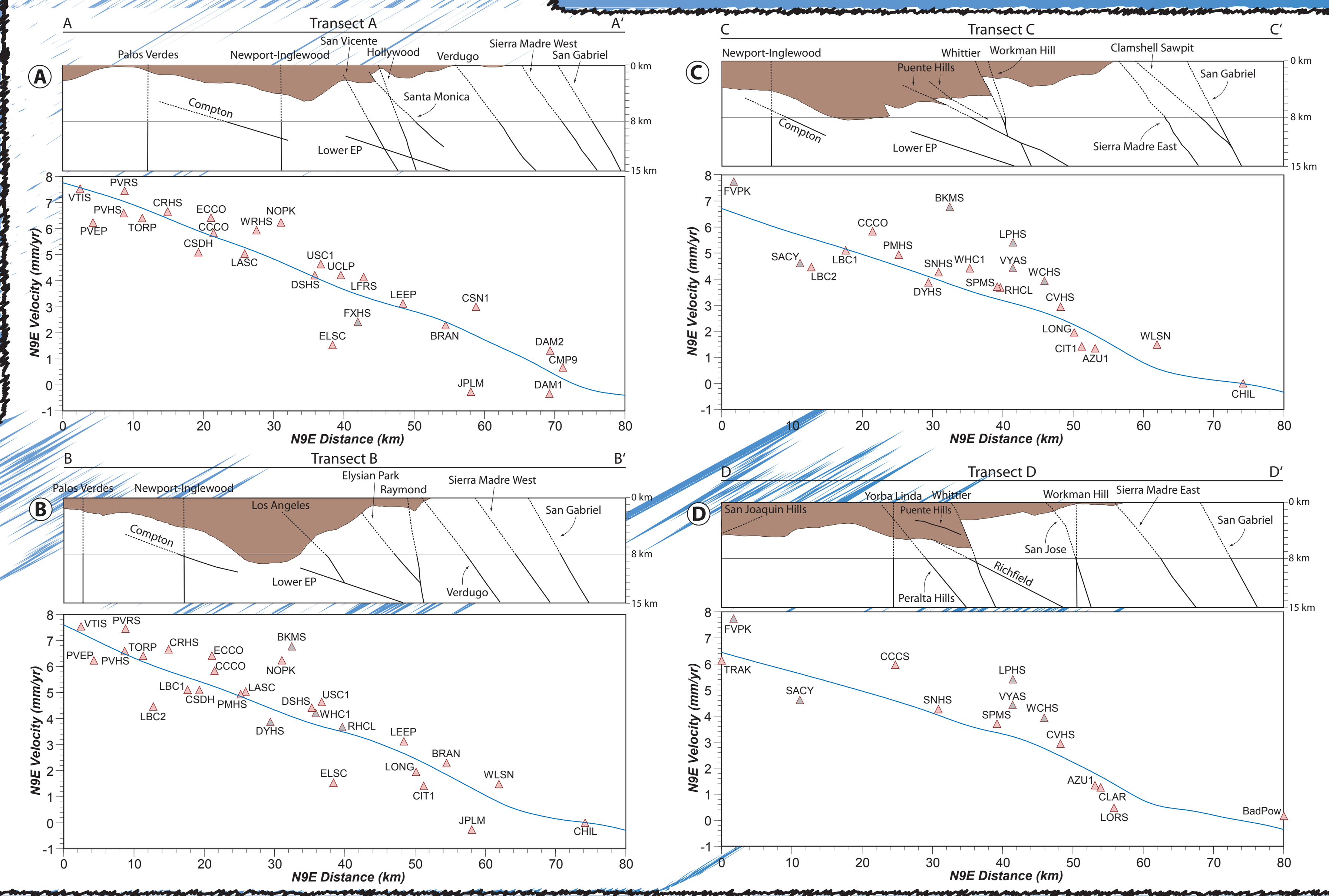

LEFT: N9°E Transects through the Los Angeles region showing model and GPS velocities. Locations of transects are shown on the figures above. A cross-sectional slice through the three-dimensional model along each transect is shown above each plot with faults shown with black lines (dashed where locked). Sedimentary basins are shaded gray. In the plots, the N9°E component of GPS velocities and station location are projected onto transects (triangles). GPS stations discussed in the text that potentially have mischaracterized anthropogenic motion are shown with gray triangles. Model results are shown with black curves. Localized convergence is strongest in the eastern transects (C and D) in both the model and GPS data.

CONCLUSIONS

Model results match well both geologic slip rate estimates and interseismic GPS velocities in the region, suggesting that the models capture the first-order features of geologic and interseismic deformation in the region. Most regions where the interseismic model produces relatively high residuals occur where GPS stations likely have mischaracterized anthropogenic and seasonal motions, suggesting that corrected GPS velocities may better elucidate the current-day tectonic deformation pattern in the Los Angeles region.
The close correlation of three-dimensional interseismic model predictions of surface velocity with geodetic data and the match of geologic model predictions of fault slip rates with geologic data suggest little discrepancy between geodetic and geologic deformation rates in the metropolitan Los Angeles region. In contrast to results from two-dimensional models of the region that evoke geologically-discrepant slip rates of 9 mm/yr on the Puente Hills fault [Argus et al., 2005], we find that steep geodetic gradients in the San Gabriel basin are matched well by a three-dimensional model with relatively fast slip on the Sierra Madre fault and relatively slow slip on the Puente Hills thrusts, in agreement with geologic slip rate estimates. Furthermore, although the models here employ homogeneous and isotropic material properties, the complex fault structure produces a heterogeneous pattern of deformation throughout the Los Angeles region, suggesting that two-dimensional analyses of the region may have limited suitability.